Heliyon 10 (2024) e29214

Contents lists available at ScienceDirect

Heliyon

journal homepage: www.cell.com/heliyon

Research article

A nomogram model of spectral CT quantitative parameters and clinical characteristics predicting lymphovascular invasion of gastric cancer

Yong-Xiu Tong [a,1], Xiao Ye [b,1], Yong-Qin Chen [c,1], Ya-ru You [d], Hui-Juan Zhang [a], Shu-Xiang Chen [a], Li-Li Wang [e,f], Yun-Jing Xue [e,f], Li-Hong Chen [e,f,*]

[a] Department of Radiology, Provincial Clinical College of Fujian Medical University, Fujian Provincial Hospital, Fuzhou, 350001, China
[b] Department of Radiology, Fujian Provincial Geriatric Hospital, Fuzhou, 350001, China
[c] Department of Pathology, Fujian Medical University Union Hospital, Fuzhou, 350001, China
[d] Department of Radiology, The First Affiliated Hospital of Zhengzhou University, Zhengzhou, 450000, China
[e] Department of Radiology, Fujian Medical University Union Hospital, Fuzhou, 350001, China
[f] Fujian Key Laboratory of Intelligent Imaging and Precision Radiotherapy for Tumors (Fujian Medical University), Fuzhou, 350001, China

ARTICLE INFO

Keywords:
Spectral computed tomography
Clinical characteristics
Gastric cancer
Lymphovascular invasion
Nomogram

ABSTRACT

Objective: The study established a nomogram based on quantitative parameters of spectral computed tomography (CT) and clinical characteristics, aiming to evaluate its predictive value for preoperative lymphovascular invasion (LVI) in gastric cancer (GC).

Methods: From December 2019 to December 2021, 171 patients with pathologically confirmed GC were retrospectively collected with corresponding clinical data and spectral CT quantitative data. Patients were divided into LVI-positive and LVI-negative groups based on their pathological results. The univariate and multivariate logistic regression analyses were used to identify the risk factors and construct a nomogram. The calibration curve and receiver operating characteristic (ROC) curve were adopted to evaluate the predictive accuracy of nomogram.

Results: Four clinical characteristics or spectral CT quantitative parameters, including Borrmann classification ($P = 0.039$), CA724 ($P = 0.007$), tumor thickness ($P = 0.031$), and iodine concentration in the venous phase (VIC) ($P = 0.004$) were identified as independent factors for LVI in GC patients. The nomogram was established based on the four factors, which had a potent predictive accuracy in the training, internal validation and external validation cohorts, with the area under the ROC curve (AUC) of 0.864 (95% CI, 0.798–0.930), 0.964 (95% CI, 0.903–1.000) and 0.877 (95% CI, 0.759–0.996), respectively.

Conclusion: This study constructed a comprehensive nomogram consisting spectral CT quantitative parameters and clinical characteristics of GC, which exhibited a robust efficiency in predicting LVI in GC patients.

* Corresponding author. Department of Radiology, Fujian Medical University Union Hospital, Fuzhou 350001, China.
E-mail address: Lihongchen01@fjmu.edu.cn (L.-H. Chen).
[1] These author contributed equal to this study.

https://doi.org/10.1016/j.heliyon.2024.e29214
Received 2 August 2023; Received in revised form 2 April 2024; Accepted 2 April 2024
Available online 3 April 2024

1. Introduction

Gastric cancer (GC) is one of the most common malignant tumors and its mortality ranks fourth among cancers worldwide [1]. Surgery is the most important treatment for early and advanced GC; however, 20–30% of patients will have local recurrence or distant metastasis after surgery [2]. Lymphovascular invasion (LVI) refers to the invasion of the tumor into lymphatic and/or blood vessels and acts as an important route for the local metastasis [3]. Regional LVI is closely associated with the recurrence of GC and the prognosis of GC patients, and LVI-positive patients have a higher recurrence rate and a worse 5-year survival rate [4,5]. Currently, GC patients are primarily stratified based on the TNM staging. Since LVI is essential for determining treatment regimen and affects the prognosis of GC patients, studies recommended that the addition of LVI to the TNM staging system might have a better efficiency for predicting the overall survival of GC patients [6,7]. However, LVI status can only be obtained after surgery, which limits its preoperative application in predicting the stage. Therefore, it is necessary to find a reliable preoperative predictive method in clinical treatment of GC.

Computed tomography (CT) is the primary examination method for the diagnosis and staging of GC. However, traditional CT can hardly identify tumor metastasis of small lymph nodes with a diameter of less than 5 mm due to the limited resolution. Emerging radiomics and deep machine learning algorithms can identify image features that are not easily observed by the naked eye to evaluate the biological characteristics of tumor and predict the prognosis of cancer patients [8,9]. However, these findings have limited repeatability and require validation by large-scale cohort.

Spectral CT is an imaging mode based on rapid switching between high-energy and low-energy X-rays, and it can produce multiple monoenergetic images and identify material decomposition [10]. Compared with regular CT, it can obtain several additional quantitative parameters. Previous studies have confirmed that spectral CT quantitative parameters exhibit superior advantages and broad prospects in early screening, preoperative staging, and predicting the prognosis of GC [11–13]. Also, studies have shown that preoperative predictive models including spectral CT are promising to assess LVI in GC patients [14,15]. However, there is no clinical characteristics of tumor [14] or standardize spectral CT quantitative parameters in their model. Multi-center data for external verification is requested too.

Since chronic inflammation is implicated to play a critical role in GC progression [16], the present study incorporated inflammatory indicators such as neutrophil-to-lymphocyte ratio (NLR) and platelet-to-lymphocyte ratio (PLR), clinical characteristics and diverse spectral CT parameters to identify potential predictive markers and establish a predictive model for LVI in GC, which will contribute to the preoperative evaluation of the prognosis of GC patients.

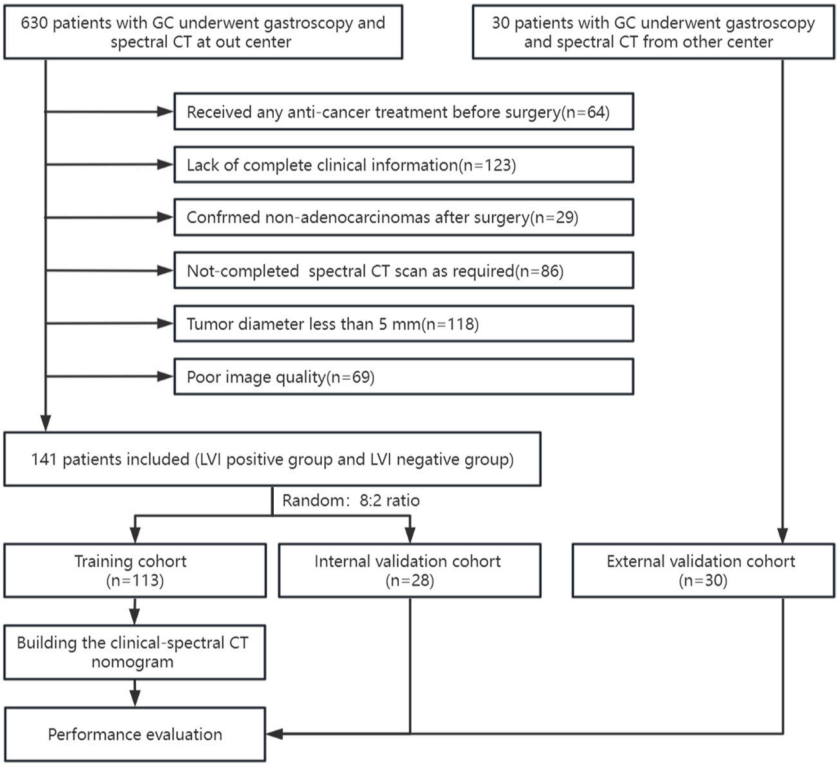

Fig. 1. Flowchart of patient's recruitment.

2. Materials and methods

The study was approved by the Ethics Committee of the Hospital and exempted from the requirement of informed consent of patients.

2.1. General information

A total of 171 GC patients between December 2019 and December 2021 were included in this study according to the following inclusion criteria: (1) pathologically confirmed GC patients with complete clinical and postoperative pathological data; (2) patients with resectable GC who received surgical resection; (3) no local or systemic treatment before surgery; and (4) dual-phase enhanced abdominal spectral CT performed within two weeks before the operation. 141 patients form Fujian Medical University Union Hospital, were identified as the primary cohort, which were randomly divided into the training cohor (N = 113) and internal validation cohort (N = 28) at a ratio of 8:2. The external validation cohort comprised 30 patients who fulfilled the selection criteria from other medical center (The First Affiliated Hospital of Zhengzhou University). The recruitment process of the study subjects is shown in Fig. 1.

2.2. Acquisition of clinical data

The clinical, serological, and pathological data of the patients were accessed through the electronic medical record system. The clinical information included age, gender and body mass index (BMI); the serological data included NLR, PLR, and tumor markers carcinoembryonic antigen (CEA), carbohydrate antigen 19-9 (CA19-9), CA724; the pathological data included the tumor location, differentiation, Lauren subtype, Borrmann classification, and LVI. Additionally, the blood serum was collected within three days before the operation.

Patients were divided into subgroups based on age (≤60 or >60 years), BMI (< 18.5, 18.5–24, or >24), serological variables including CEA (≥5.0 or < 5.0 ng/ml), CA19-9 (≥37.0 or < 37.0 U/mL), and CA724 (≥6.9 or < 6.9 U/mL), and tumor differentiation (poor or good), where poorly differentiated or undifferentiated tumor was classified as poor differentiation group, well differentiated and moderately differentiated tumor was classified as good differentiated group, and the tumor with unclear differentiation were classified by pathological consultation.

2.3. CT scan

The CT scans from the top of the diaphragm to the upper edge of the pubic symphysis, and the patient was told to take the supine position and hold his breath at the end of inspiration before the examination. The 256-slice GE Revolution CT gemstone spectral imaging (GSI) was used with a voltage of 80 kV/140 kV, a current of 485 mA, a pitch of 0.992:1, a slice thickness of 5 mm, an interslice interval of 5 mm, and a reconstruction slice thickness of 1.25 mm. During contrast-enhanced scanning, 400 mgI/ml of nonionic agent was injected at a flow rate of 2.0–2.5 ml/s and a dose of 1.0–1.5 ml/kg. The arterial phase scan was automatically triggered when the CT value of the abdominal aorta reached 150 HU, and the venous phase scan was initiated 28 s later to obtain the raw spectral data of the arterial and venous phases.

2.4. CT image analysis and spectral parameter acquisition

The obtained raw data were analyzed using GE post-processing workstation ADW4.7. Two radiologists (with more than five and ten years of working experience, respectively) who were unknown to the pathological results independently review the images in the GSI viewer and processed the data. When drawing the region of interest (ROI) along the tumor edge at the largest level of the tumor, the necrotic area was avoided. Iodine concentration (IC) in the arterial phase (AIC) and the venous phase (VIC), and 40 Kev and 70 Kev single-energy CT values were obtained on the iodine-based and single-energy images. A circular ROI was placed on the abdominal aorta at the same scanning level to calculate the normalized iodine concentration (nIC) in the arterial phase (AnIC) and the venous phase (VnIC), the slope (K) of the energy spectrum curve in the venous phase (VK), the difference between AIC and VIC (AVIC), and the difference between AnIC and VnIC (AVnIC). The ROI was placed in the same size, shape, and position during different phases. To obtain the IC and nIC of peritumoral fat in the venous phase (FVIC and FVnIC), the ROI of peritumoral fat was delineated at the largest level of the tumor in the venous phase and kept about 2 mm away from the tumor margin. The K was calculated as the ratio of (CT 40Kev - CT 70kev) to (70-40); the nIC was calculated as the ratio of lesion IC to abdominal aorta IC; the AVIC was calculated as the VIC minus the AIC; the AVnIC was calculated as the VnIC minus the AnIC.

2.5. Statistical analysis

IBM SPSS Statistics 28.0, Python 3.8.8, and R 4.0.3 were used for data analysis and visualization. For continuous variables, Kolmogorov-Smirnov test was used for the normality hypothesis test. They were presented as mean ± standard deviation (SD) and were compared using the student's t or Mann-Whitney *U* test. The categorical variables were compared using the χ^2 or Fisher's exact test. The univariate logistic regression analysis was used to screen independent variables that were associated with LVI of GC, and those significant ones were subjected to the multivariate regression analysis. The least absolute shrinkage and selection operator (LASSO) algorithm was used to process the collinearity of the spectrum CT quantitative parameters. The nomogram predictive model

was established consisting of obtained independent factors of LVI. The performance of the nomogram was evaluated using the calibration curve and the area under the receiver operating characteristic (ROC) curve (AUC). The nomogram, AUC, and calibration curve were drawn by the "RMS" R package. A two-sided P value < 0.05 suggested a statistically significant difference.

3. Results

3.1. Clinical and pathological characteristics of patients

A total of 171 GC patients were enrolled according to the inclusion criteria, including 119 males and 52 females. Their age ranged from 28 to 80 (62.33 ± 8.76) years. The clinical characteristics of the training, internal validation and external validation cohorts are shown in Table 1. The positive rate of LVI was 53.9%, 57.1% and 60.0% in the training, internal and external validation cohort, respectively. Also, clinical characteristics were comparable among the three groups. Of these patients, 95 were positive for LVI and 76 were negative. The clinical characteristics of LVI-positive and LVI-negative groups in the training, internal and external validation cohorts are shown in Table 2. In the LVI-positive group of training, internal and external validation cohorts, there were more patients with poor differentiation and Borrmann type III-IV GC, but fewer patients had the Lauren intestinal subtype. Additionally, CA724, CA19-9, NLR, and PLR levels were significantly higher in the LVI-positive group than those in the LVI-negative group. After that, univariate logistic regression analysis identified that among the above clinical characteristics, tumor differentiation, Lauren subtype, Borrmann classification, NLR, PLR, CA19-9, and CA724 level were significantly correlated with LVI ($P < 0.05$).

3.2. Spectral CT parameters

The spectral CT quantitative parameters are shown in Table 3. In training, internal and external validation cohorts, the tumor thickness and spectral CT quantitative parameters were significantly higher in the LVI-positive group (Fig. 2:A-D) than those in the LVI-negative group (Fig. 3:A-D) ($P < 0.05$). The heatmap of correlation analysis showed notable collinearity among the spectral CT quantitative parameters (Fig. 4). Therefore, the LASSO algorithm was adopted to exclude parameters with collinearity and identify that AnIC, VIC, FVIC, and AVIC were highly correlated with LVI (Fig. 5:A-B).

3.3. Construction of the predictive model

Then, those crucial clinical characteristics and spectral CT quantitative parameters were subjected to the multivariate logistic regression analysis to construct a predictive model. The result showed that Borrmann classification ($P = 0.039$), CA724 ($P = 0.007$),

Table 1
Clinical characteristics of the training and validation cohorts.

Characteristics		Training cohort (n = 113)	Internal validation cohort (n = 28)	External validation cohort (n = 30)
Sex	male	79 (69.9%)	19 (67.9%)	21 (70.0%)
	female	34 (30.1%)	9 (32.1%)	9 (30.0%)
Age (years)	≤60	42 (37.2%)	9 (32.1%)	11 (36.7%)
	> 60	71 (62.8%)	19 (67.9%)	19 (63.3%)
BMI	< 18.5	4 (3.5%)	1 (3.6%)	0 (0%)
	18.5–24	58 (51.3%)	14 (50.0%)	16 (53.3%)
	> 24	51 (45.2%)	13 (46.4%)	14 (46.7%)
CEA (ng/mL)	≥5.0	22 (19.5%)	9 (32.2%)	6 (20.0%)
	< 5.0	91 (80.5%)	19 (67.8%)	24 (80.0%)
CA19-9 (U/mL)	≥37.00	20 (17.7%)	5 (17.9%)	6 (20.0%)
	< 37.00	93 (82.3%)	23 (82.1%)	24 (80.0%)
CA724 (U/mL)	≥6.90	22 (19.5%)	7 (25.0%)	7 (23.3%)
	< 6.90	91 (80.5%)	21 (75.0%)	23 (76.7%)
NLR		2.46 ± 1.55	2.45 ± 1.73	2.74 ± 0.26
PLR		171.82 ± 94.53	160.98 ± 89.69	164.34 ± 59.34
Tumor location	Cardia/Fundus	23 (20.35%)	11 (39.3%)	9 (30.0%)
	Body	44 (38.94%)	7 (25.0%)	8 (26.7%)
	Antrum	34 (30.09%)	6 (21.4%)	9 (30.0%)
	≥2/3 stomach	12 (10.62%)	4 (14.3%)	4 (13.3%)
Differentiation	Good	47 (41.6%)	18 (64.3%)	13 (43.3%)
	Poor	66 (58.4%)	10 (35.7%)	17 (56.7%)
Lauren subtype	Intestinal	55 (48.7%)	17 (60.7%)	13 (43.3%)
	Mixed	22 (19.5%)	5 (17.9%)	9 (30.0%)
	Diffused	36 (31.8%)	6 (21.4%)	8 (26.7%)
Borrmann classification	I-II	60 (53.1%)	14 (50.0%)	16 (53.3%)
	III-IV	53 (46.9%)	14 (50.0%)	14 (46.7%)
LVI	Positive	61 (53.9%)	16 (57.1%)	18 (60.0%)
	Negative	52 (46.1%)	12 (42.9%)	12 (40.0%)

CEA, Carcinoembryonic antigen; CA19−9, Carbohydrate antigen 19-9; CA724,Carbohydrate antigen 724; NLR, neutrophil-to-lymphocyte ratio; PLR, platelet-to-lymphocyte ratio; LVI, Lymphovascular invasion.

Table 2
Comparison of clinicopathological characteristics of LVI-positive and LVI-negative groups in the training and validation cohorts.

Characteristics		Training cohort			Internal validation cohort			External validation cohort		
		LVI(+) (n = 61)	LVI(−) (n = 52)	P value	LVI(+) (n = 16)	LVI(−) (n = 12)	P value	LVI(+) (n = 18)	LVI(−) (n = 12)	P value
Sex	male	41 (67.2%)	38 (73.1%)	0.499	11 (68.8%)	8 (66.7%)	0.583	13 (72.2%)	8 (66.7%)	0.599
	female	20 (32.8%)	14 (26.9%)		5 (31.2%)	4 (33.3%)		5 (27.8%)	4 (33.3%)	
Age (years)	≤60	23 (37.7%)	19 (36.5%)	0.898	5 (31.2%)	4 (33.3%)	0.636	6 (33.3%)	5 (41.7%)	0.837
	> 60	38 (62.3%)	33 (63.5%)		11 (68.8%)	8 (66.7%)		12 (66.7%)	7 (58.3%)	
BMI	< 18.5	3 (4.9%)	1 (1.9%)	0.671	0 (0%)	1 (8.3%)	0.051	0 (0%)	0 (0%)	0.082
	18.5–24	30 (49.2%)	28 (53.8%)		8 (50.0%)	6 (50.0%)		10 (55.6%)	6 (50.0%)	
	> 24	28 (45.9%)	23 (44.3%)		8 (50.0%)	5 (41.7%)		8 (44.4%)	6 (50.0%)	
CEA (ng/mL)	≥5.0	14 (23.0%)	8 (15.4%)	0.314	8 (50.0%)	1 (8.3%)	0.064	3 (16.7%)	3 (25.0%)	0.311
	< 5.0	47 (77.0%)	44 (84.6%)		8 (50.0%)	11 (91.7%)		15 (83.3%)	9 (75.0%)	
CA19-9 (U/mL)	≥37.00	17 (27.9%)	3 (5.8%)	0.005*	5 (31.2%)	0 (0%)	0.057	4 (22.2%)	2 (16.7%)	0.172
	< 37.00	44 (72.1%)	49 (94.2%)		11 (68.8%)	12 (100%)		14 (77.8%)	10 (83.3%)	
CA724 (U/mL)	≥6.90	21 (34.4%)	1 (1.9%)	0.002*	6 (37.5%)	1 (8.3%)	0.046*	6 (33.3%)	1 (8.3%)	0.033*
	< 6.90	40 (65.6%)	51 (98.1%)		10 (62.5%)	11 (91.7%)		12 (66.7%)	11 (91.7%)	
NLR		2.83 ± 2.15	2.09 ± 0.95	0.037*	2.81 ± 1.92	2.09 ± 1.47	0.024*	2.74 ± 3.69	2.22 ± 2.85	0.047*
PLR		189.68 ± 89.97	153.95 ± 98.52	0.049*	198.24 ± 105.92	122.97 ± 30.22	0.032*	173.75 ± 94.67	149.85 ± 103.17	0.029*
Tumor location	Cardia/ Fundus	11 (18.0%)	12 (23.1%)	0.751	8 (50.0%)	3 (25.0%)	0.057	5 (27.8%)	4 (33.3%)	0.833
	Body	23 (37.7%)	21 (40.4%)		3 (18.8%)	4 (33.3%)		5 (27.8%)	3 (25.0%)	
	Antrum	19 (31.1%)	15 (28.8%)		3 (18.8%)	3 (25.0%)		6 (33.3%)	3 (25.0%)	
	≥2/3 stomach	8 (13.2%)	4 (7.7%)		2 (12.4%)	2 (16.7%)		2 (11.1%)	2 (16.7%)	
Differentiation	Good	17 (27.9%)	30 (57.7%)	0.002*	8 (50.0%)	10 (83.3%)	0.035*	8 (44.4%)	5 (41.7%)	0.051
	Poor	44 (72.1%)	22 (42.3%)		8 (50.0%)	2 (16.7%)		10 (55.6%)	7 (58.3%)	
Lauren subtype	Intestinal	22 (36.1%)	33 (63.5%)	0.016*	6 (37.6%)	11 (91.7%)	< 0.001*	5 (27.8%)	8 (66.6%)	0.037*
	Mixed	15 (24.6%)	7 (13.4%)		5 (31.2%)	0		7 (38.9%)	2 (16.7%)	
	Diffused	24 (39.3%)	12 (23.1%)		5 (31.2%)	1 (8.3%)		6 (33.3%)	2 (16.7%)	
Borrmann classification	I-II	23 (37.7%)	37 (71.2%)	< 0.001*	3 (18.8%)	11 (91.7%)	< 0.001*	7 (38.9%)	9 (75.0%)	< 0.001*
	III-IV	38 (62.3%)	15 (28.8%)		13 (81.2%)	1 (8.3%)		11 (61.1%)	3 (25.0%)	

LVI, Lymphovascular invasion; CEA, Carcinoembryonic antigen; CA19−9, Carbohydrate antigen 19-9; CA724, Carbohydrate antigen 724; NLR, neutrophil-to-lymphocyte ratio.
PLR, platelet-to-lymphocyte ratio.

Table 3
Comparison of spectral CT quantitative parameters of LVI-positive and LVI-negative groups in the training and validation cohorts.

Parameters	Training cohort			Internal validation cohort			External validation cohort		
	LVI(+) (n = 61)	LVI(−) (n = 52)	P value	LVI(+) (n = 16)	LVI(−) (n = 12)	P value	LVI(+) (n = 18)	LVI(−) (n = 12)	P value
Tumor thickness (mm)	15.44 ± 4.84	11.15 ± 4.54	<0.001	16.06 ± 0.64	10.17 ± 2.86	<0.001	17.01 ± 0.31	13.58 ± 1.63	<0.001
AIC (100 μg/ml)	18.23 ± 5.90	15.87 ± 5.66	0.038	21.04 ± 5.21	16.25 ± 4.83	0.033	19.17 ± 4.06	14.33 ± 5.02	0.021
AnIC	0.17 ± 0.07	0.14 ± 0.05	0.046	0.20 ± 0.07	0.15 ± 0.04	0.041	0.18 ± 1.01	0.14 ± 0.81	0.039
VIC (100 μg/ml)	23.52 ± 5.73	18.15 ± 5.04	<0.001	24.89 ± 4.49	17.96 ± 4.86	<0.001	23.51 ± 2.57	17.99 ± 3.92	<0.001
VnIC	0.56 ± 0.14	0.47 ± 0.13	0.002	0.58 ± 0.11	0.45 ± 0.11	0.028	0.55 ± 0.60	0.46 ± 0.51	0.007
VK	4.45 ± 1.09	3.44 ± 0.96	<0.001	4.63 ± 0.84	3.36 ± 0.95	<0.001	4.36 ± 1.42	2.99 ± 1.17	<0.001
AVIC (100 μg/ml)	5.26 ± 6.49	2.28 ± 4.02	0.008	3.85 ± 7.14	1.86 ± 2.28	0.014	5.02 ± 4.99	2.05 ± 0.02	0.031
AVnIC	0.39 ± 0.15	0.33 ± 0.11	0.018	0.38 ± 0.12	0.30 ± 0.09	0.023	0.33 ± 0.48	0.23 ± 0.55	0.002
FVIC (100 μg/ml)	−3.84 ± 5.71	−7.56 ± 4.36	<0.001	0.55 ± 6.00	−5.38 ± 4.82	<0.001	−2.26 ± 3.61	−6.62 ± 3.09	<0.001
FVnIC	−0.10 ± 0.15	−0.20 ± 0.12	<0.001	0.02 ± 0.14	−0.14 ± 0.13	<0.001	0.00 ± 0.26	−0.28 ± 0.37	<0.001

LVI, Lymphovascular invasion; AIC, Iodine concentration in the arterial phase; AnIC, normalized iodine concentration in the arterial phase; VIC, Iodine concentration in the venous phase; VnIC, normalized iodine concentration in the venous phase; VK, the slope (K) of the energy spectrum curve in the venous phase; AVIC, the difference between AIC and VIC; AVnIC, the difference between AnIC and VnIC; FVIC, Iodine concentration peritumoral fat in the venous phase; FVnIC, normalized iodine concentration of peritumoral fat in the venous.

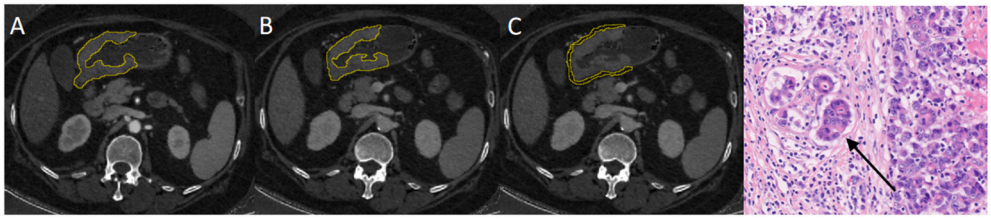

Fig. 2. A 70 years old female patient with pathologically confirmed gastric adenocarcinoma, staging of pT4aN3aM0, LVI positive. The tumor thickness was 21 mm, Borrmann classification of III. (A) Iodine map at arterial phase, IC value was 21.17 (100 mg/ml); (B) Iodine map at venous phase, IC value was 30.68 (100 mg/ml); (C) Iodine map of peritumoral fat at venous phase, IC value was 2.80 (100 mg/ml); (D) The histopathology (HE, magnification: × 200) showed adenocarcinomas cells infiltrate into lymphovascular structure (arrow).

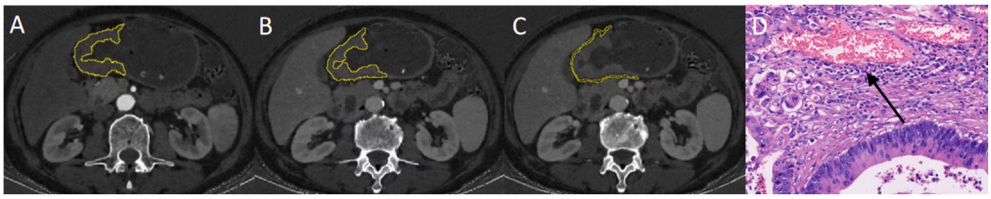

Fig. 3. A 68 years old male patient with pathologically confirmed gastric adenocarcinoma, staging of pT3N0M0, LVI negative. The tumor thickness was 20.8 mm, Borrmann classification of II. (A) Iodine map at arterial phase, IC value was 22.01 (100 mg/ml); (B) Iodine map at venous phase, IC value was 30.53 (100 mg/ml); (C) Iodine map of peritumoral fat at venous phase, IC value was 1.78 (100 mg/ml); (D) The histopathology (HE, magnification: × 200) showed normal lymphovascular structure (arrow).

tumor thickness ($P = 0.031$), and VIC ($P = 0.004$) were independent factors for LVI in GC patients (Table 4). A nomogram composed of the four factors was further established (Fig. 6).

3.4. Efficiency of the predictive model

The AUC and calibration curve were used to evaluate the performance of the nomogram model. The AUC of nomogram model to identify LVI in the training, internal and external validation cohorts was 0.864 (95% CI, 0.798–0.930), 0.964 (95% CI, 0.903–1.000) and 0.877 (95% CI, 0.759–0.996), respectively, indicating that the model had a potent discriminatory ability (Fig. 7:A-C). The calibration curve for the nomogram model in the training, internal and external validation cohorts was shown in (Fig. 8:A-C). The calibration curve basically aligned with the ideal curve with a high degree of calibration, indicating that the model had a high feasibility in predicting LVI in GC patients.

4. Discussion

The present study constructed a preoperative nomogram model for predicting LVI of GC patients based on spectral CT quantitative parameters and clinical characteristics. The model contained four independent predictors, including Borrmann classification, CA724, tumor thickness, and VIC, which provided a simple and effective method for predicting LVI and the prognosis of GC patients.

Among enrolled 171 GC patients, the incidence of LVI was 55.6%, which was consistent with previous research [17]. The connection between the tumor and surrounding vessels, lymphatics, and nerves plays a vital role in tumor occurrence and development. Tumor can metastasize to distant organs through blood vessels or lymphatics. Therefore, GC cases with a higher tumor thickness and Borrmann invasive type are more likely to develop LVI. Numerous studies have shown that the tumor thickness and Borrmann classification are significantly different between LVI-positive and LVI-negative groups in GC patients [2,18,19]. Consistent with previous finding, our study revealed that the probability of LVI increased by 2.804-fold with invasive type of Borrmann classification and higher tumor thickness. Moreover, a Japanese study showed that tumor differentiation was associated with lymph node metastasis [20], which was consistent with our finding that tumor differentiation was associated with LVI of GC. However, this finding was discrepant with that of Li et al. [14], which might be due to the different grouping strategy. Li et al. divided the tumor differentiation into good, moderate, and poor differentiation, whereas our study only divided it into good and poor differentiation.

Studies have proposed several serological indicators that are associated with the metastasis and prognosis of GC. The present study included NLR, PLR, CA19-9, and CA724 and showed that all serological indicators except for CEA were the potential predictors of LVI. Although previous studies suggested a correlation between CEA and LVI in GC patients [15,17], which was inconsistent with our findings, it should be noted that CEA was widely expressed in the body and its level was easily affected by factors other than tumors. Chronic inflammation is implicated to play a critical role in GC development and NLR and PLR are inflammatory indicators [21]. Inflammation produces a variety of cytokines including vascular endothelial growth factor (VEGF) and interluckeukin-8 (IL-8) which promote tumor angiogenesis and distant metastasis [22]. Herein, our study showed that NLR and PLR had a strong correlation with

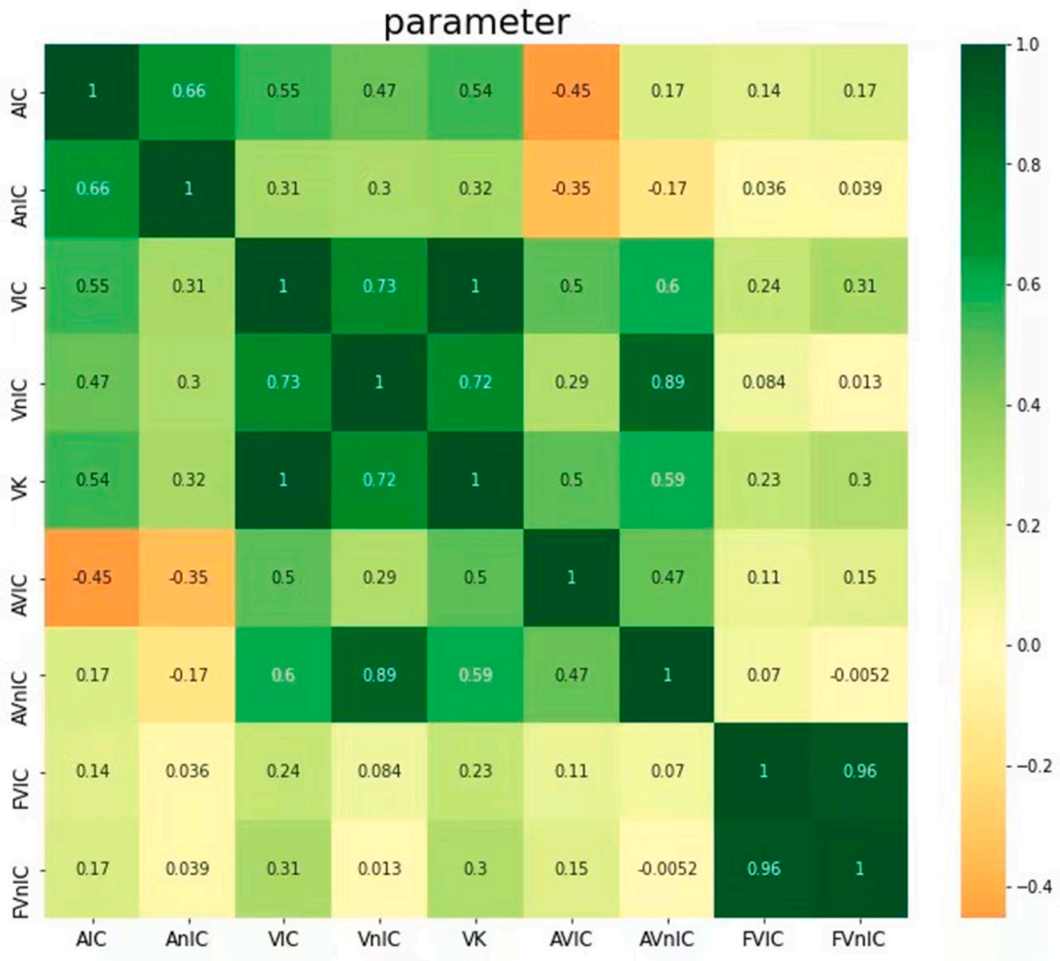

Fig. 4. Correlation coefficient heatmap. Abscissa and ordinate for each spectrum parameter, the deeper the color represents the correlation coefficient is larger.

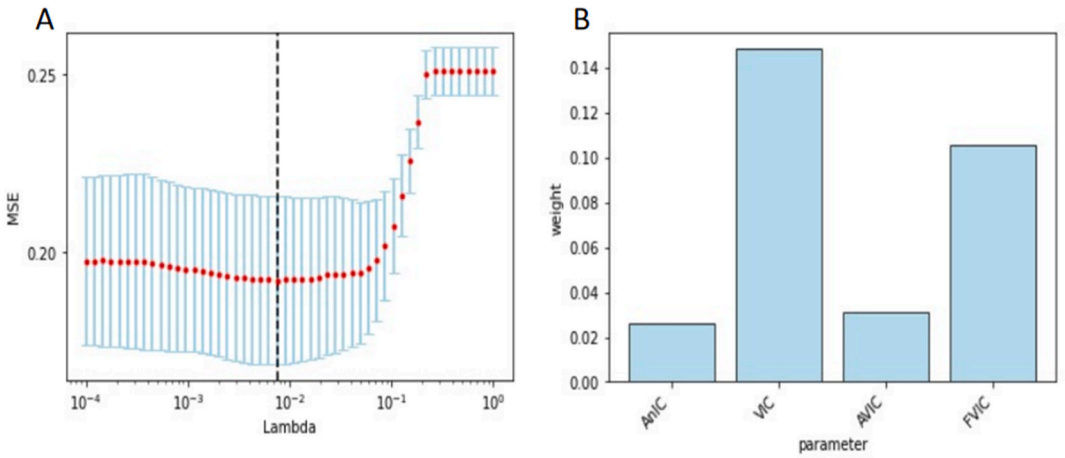

Fig. 5. (A) CV cartogram. The x-coordinate is the log of the penalty function; The y-coordinate is the MSE (mean squared error); When the mean square error reaches the minimum, the penalty function is the optimal solution. (B)Parameter weight bar chart. The x-coordinate is the parameter after lasso; The y-coordinate is the weight of parameter.

Table 4
Risk factors for lymphovascular invasion in gastric cancer.

Variable	Nomogram					
	β	SE	Wald ×2	OR	95%CI	P value
Borrmann classification	1.031	0.500	4.247	2.804	1.052–7.478	0.039
Tumor thickness	0.116	0.054	4.643	1.123	1.001–1.248	0.031
CA724	2.895	1.081	7.170	18.092	2.173–150.640	0.007
VIC	0.153	0.052	8.508	1.165	1.051–1.291	0.004

CA724,Carbohydrate antigen 724; VIC, Iodine concentration in the venous phase.

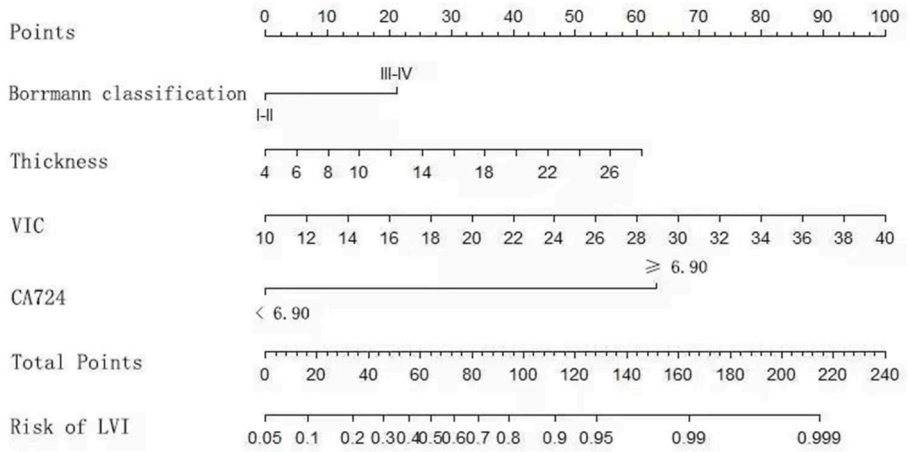

Fig. 6. The Clinical-spectral CT model for predicting LVI of GC patients. A nomogram scaled by the coefficient of each factor.

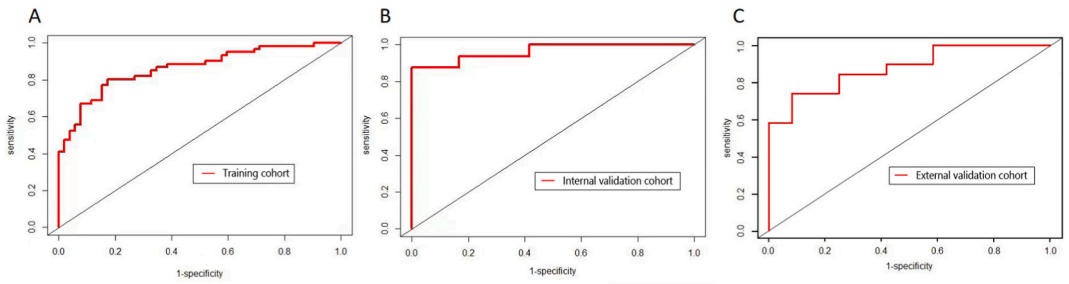

Fig. 7. The receiver operation characteristic curve for predicting LVI of GC patients in the training cohort(A), internal validation cohort (B) and external validation cohort(C).

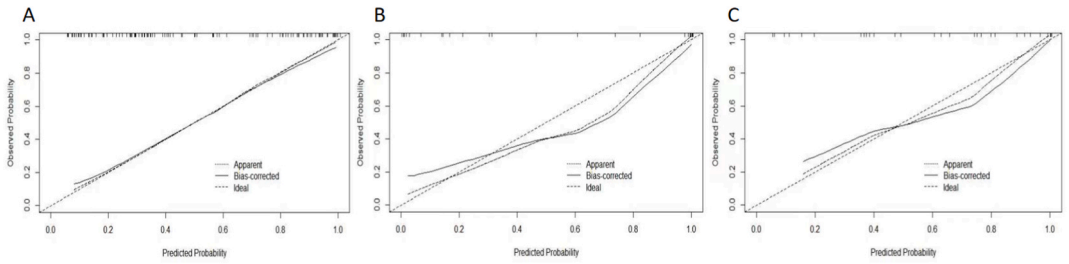

Fig. 8. The calibration curve demonstrating predictions from the model to the actual observed probability in the training cohort (A), internal validation cohort (B) and external validation cohort(C).

LVI. At present, several tumor markers, such as CEA, CA19-9 and CA724 have been widely used in the diagnosis, prognosis evaluation, and efficacy testing of patients with GC [23,24]. Moreover, CA724 had the highest diagnostic efficiency and it is associated with tumor biological behavior such as tumor size, depth of invasion, stage and lymph node involvement [25]. Therefore, CA724 level are effective in evaluating the presence of LVI in GC, and was included in the nomogram model. Ren et al. proposed that CA125 was an independent factor for LVI in GC [15], but in our study, it was not included in the nomogram model. Therefore, more comprehensive data and multiple indicators were required to construct the predictive model with the optimal diagnostic efficiency. It is widely known that spectral CT quantitative parameters can predict lymph node metastasis in GC [26,27], which was consistent with our finding that some spectral quantitative parameters were highly correlated with LVI. As a result, VIC was an independent risk factor of LVI increased the probability of LVI by 1.165-fold for every unit increase in its value, which was consistent with the previous study [2]. LVI was primarily caused by tumor-induced angiogenesis and incomplete wall of new blood vessels, which allowed cancer cells to easily invade into the blood vessels. The iodine contrast agent can penetrate and temporarily reside in the blood vessels during the arterial phase; at the venous phase, the level of iodine in the tumor vessels is at a balanced status. Since the excretion rate of the iodine contrast agent slows down during the venous phase, more contrast agents will exist in the tumor stroma through the incomplete blood vessel walls, therefore, the VIC can portend the tumor neovascularization [28,29]. However, Jing et al. indicated that IC in the delayed phase (ICDP) was the best predictor for LVI [14], primarily due to different administration strategies of contrast enhancement. They adopt a three-phase enhancement scheme, whereas our study used a two-phase one, which was consistent with most previous studies [15,30]. Additionally, some studies have proposed that VnIC could reduce the impact of individual circulatory differences and exhibited better sensitivity and specificity than VIC [31–33], which was inconsistent with our findings, possibly due to different scanning methods. The arterial phase scanning was triggered by detecting the CT value of the abdominal aorta, so that the nIC was able to reduce the impact of individual circulatory differences. However, the iodine contrast agent in the abdominal aorta remained high during the venous phase, which might affect the calculation of nIC and led to a wrong value of nIC, as previously reported [34]. Therefore, the calculation method and application of the nIC should be carefully evaluated in further studies.

The FVIC was rarely included in previous models. Our results indicated that it had a significant impact on GC development. The contact surface between the tumor and the perigastric lymphatic vessels will increase if GC penetrates the serosal membrane, which increase the possibility of LVI. Nevertheless, GC is frequently accompanied by serosal inflammatory reactions, which exhibits unclear boundaries and blurred fat space on CT scanning, which may be mistaken for the involvement of the serosal membrane by tumor. Zhou et al. proposed that iodine contrast agent could enter the adipose tissue when the membrane of thymic tumors was destroyed, resulting in an increased IC in peritumoral fat. Therefore, measuring IC in peritumoral fat could predict lymph node metastasis and vascular tumor thrombus [35]. Our study also conveyed a strong association between the FVIC and LVI in GC.

Compared with Ren et al.'s model [14], our model appears simple, quantitative and easy to use, it is superior to any other model with relatively high AUCs of 0.864 and 0.964 in primary and validation dataset. These findings support the selection of variables for model development is reasonable and feasible. Furthermore, the predictive efficacy of the nomoram was externally validated in a prospective cohort, with relatively high AUCs of 0.877, suggestive of its good generalization.

The study had some limitations. First, the sample size was relatively small, and more patients should be recruited to confirm the findings in this study. Second, the lack of TNM staging system data and some clinical data such as helicobacter pylori (HP) and CA125 and the truncation of some indicators could result in a selection bias, which might affect the predictive potency of the nomogram model. Additional studies incorporating more comprehensive factors are needed to better predict the LVI in GC. Finally, the GC lesion enhancement may be affected by the volume and rate of the contrast agent administration, which may affect the experimental results.

In summary, the present study identified spectral CT quantitative parameters and clinical characteristics that were associated with LVI and constructed a corresponding predictive model, which exhibited a potent efficiency in discriminating LVI. Our model would provide a potential strategy for predicting LVI in GC patients.

Data availability statement

Data included in article/supp. Material/referenced in article.

Funding statement

This study was supported by the Startup Fund for scientific research, Fujian Medical University (No.2019QH1042).

Ethics

This study was approved by the Ethics Committee for Clinical Investigation of Fujian Medical University, China (N0.2022KJT016). Written informed consent from all patients was exempted because of retrospective study.

CRediT authorship contribution statement

Yong-Xiu Tong: Writing – review & editing, Writing – original draft, Formal analysis, Data curation, Conceptualization. **Xiao Ye:** Writing – review & editing, Writing – original draft, Formal analysis, Data curation, Conceptualization. **Yong-Qin Chen:** Writing – review & editing, Writing – original draft, Formal analysis, Data curation, Conceptualization. **Ya-ru You:** Formal analysis, Data curation. **Hui-Juan Zhang:** Validation, Supervision, Investigation. **Shu-Xiang Chen:** Software, Formal analysis. **Li-Li Wang:**

Validation, Supervision. **Yun-Jing Xue:** Validation, Supervision, Project administration. **Li-Hong Chen:** Visualization, Validation, Supervision, Project administration, Funding acquisition, Conceptualization.

Declaration of competing interest

The authors declare that they have no known competing financial interests or personal relationships that could have appeared to influence the work reported in this paper.

References

[1] H. Sung, J. Ferlay, R.L. Siegel, M. Laversanne, I. Soerjomataram, A. Jemal, et al., Global cancer statistics 2020: GLOBOCAN estimates of incidence and mortality worldwide for 36 cancers in 185 countries, CA: a cancer journal for clinicians 71 (2021) 209–249.

[2] Y. Meng, X. Huang, J. Liu, J. Chen, Z. Bu, G. Wu, et al., A novel nomogram for individually predicting of vascular invasion in gastric cancer, Technol. Cancer Res. Treat. 20 (2021) 15330338211004924.

[3] E. Kikuchi, V. Margulis, P.I. Karakiewicz, M. Roscigno, S. Mikami, Y. Lotan, et al., Lymphovascular invasion predicts clinical outcomes in patients with node-negative upper tract urothelial carcinoma, J. Clin. Oncol. 27 (2009) 612.

[4] S. Choi, W.J. Hyung, ASO author reflections: lymphovascular invasion has a similar prognostic value as lymph node involvement in patients with early gastric cancer, Ann. Surg Oncol. 28 (2021) 8936, 8936.

[5] S. Choi, J.H. Song, S. Lee, M. Cho, Y.M. Kim, H.-I. Kim, et al., Lymphovascular invasion: traditional but vital and sensible prognostic factor in early gastric cancer, Ann. Surg Oncol. 28 (2021) 8928–8935.

[6] H. Osumi, H. Kawachi, K. Murai, K. Kusafuka, S. Inoue, M. Kitamura, et al., Risk stratification for lymph node metastasis using Epstein–Barr virus status in submucosal invasive (pT1) gastric cancer without lymphovascular invasion: a multicenter observational study, Gastric Cancer 22 (2019) 1176–1182.

[7] J. Lu, Y. Dai, J.-W. Xie, J.-B. Wang, J.-X. Lin, Q.-Y. Chen, et al., Combination of lymphovascular invasion and the AJCC TNM staging system improves prediction of prognosis in N0 stage gastric cancer: results from a high-volume institution, BMC Cancer 19 (2019) 1–9.

[8] Q. Guo, Q. Sun, X. Bian, M. Wang, H. Dong, H. Yin, et al., Development and validation of a multiphase CT radiomics nomogram for the preoperative prediction of lymphovascular invasion in patients with gastric cancer, Clin. Radiol. 8 (2023) e552–e559.

[9] L. Fan, J. Li, H. Zhang, H. Yin, R. Zhang, J. Zhang, et al., Machine learning analysis for the noninvasive prediction of lymphovascular invasion in gastric cancer using PET/CT and enhanced CT-based radiomics and clinical variables, Abdominal Radiology 47 (2022) 1209–1222.

[10] D.A. Steffen, L. Suter-Magpantay, F. Adomat, S. Blöchlinger, L. Weber, Beyond greyscale: improved detection of myocardial perfusion defects in spectral CT aortic angiography, European Heart Journal-Cardiovascular Imaging 24 (2023) e95, e95.

[11] C. Shi, Y. Yu, J. Yan, C. Hu, The added value of radiomics from dual-energy spectral CT derived iodine-based material decomposition images in predicting histological grade of gastric cancer, BMC Med. Imag. 22 (2022) 173.

[12] S.-M. Cheng, W. Ling, J. Zhu, J.-R. Xu, L.-M. Wu, H.-X. Gong, Dual energy spectral CT imaging in the assessment of gastric cancer and cell proliferation: a preliminary study, Sci. Rep. 8 (2018) 17619.

[13] R. Wang, J. Li, M. Fang, D. Dong, P. Liang, J. Gao, The value of spectral CT-based radiomics in preoperative prediction of lymph node metastasis of advanced gastric cancer, Zhonghua Yixue Zazhi 100 (2020) 1617–1622.

[14] J. Li, Y. Wang, R. Wang, J.-b. Gao, J.-r. Qu, Spectral CT for preoperative prediction of lymphovascular invasion in resectable gastric cancer: with external prospective validation, Front. Oncol. 12 (2022) 942425.

[15] T. Ren, W. Zhang, S. Li, L. Deng, C. Xue, Z. Li, et al., Combination of clinical and spectral-CT parameters for predicting lymphovascular and perineural invasion in gastric cancer, Diagnostic Interventional Imaging 103 (2022) 584–593.

[16] J. Sun, X. Chen, P. Gao, Y. Song, X. Huang, Y. Yang, et al., Can the neutrophil to lymphocyte ratio be used to determine gastric cancer treatment outcomes? A systematic review and meta-analysis, Dis. Markers 2016 (2016) 7862469.

[17] F. Zhang, H. Chen, D. Luo, Z. Xiong, X. Li, S. Yin, et al., Lymphovascular or perineural invasion is associated with lymph node metastasis and survival outcomes in patients with gastric cancer, Cancer Med. 12 (2023) 9401–9408.

[18] J. Liu, H. Li, P. Zhou, T. Cai, Z. Tang, Y. Wang, et al., Reevaluation of lymphovascular invasion in gastric cancer using endothelial markers D2-40 and EVG: enhanced detection, better predictor of lymph node metastasis and biological aggressiveness, J. Surg. Oncol. 123 (2021) 1736–1741.

[19] X. Chen, Z. Yang, J. Yang, Y. Liao, P. Pang, W. Fan, et al., Radiomics analysis of contrast-enhanced CT predicts lymphovascular invasion and disease outcome in gastric cancer: a preliminary study, Cancer Imag. 20 (2020) 1–12.

[20] H. Saito, Y. Fukumoto, T. Osaki, Y. Yamada, K. Fukuda, S. Tatebe, et al., Prognostic significance of the ratio between metastatic and dissected lymph nodes (n ratio) in patients with advanced gastric cancer, J. Surg. Oncol. 97 (2008) 132–135.

[21] T. Toyokawa, K. Muguruma, M. Yoshii, T. Tamura, K. Sakurai, N. Kubo, et al., Clinical significance of prognostic inflammation-based and/or nutritional markers in patients with stage III gastric cancer, BMC Cancer 20 (2020) 1–14.

[22] Y.J. Jung, J.S. Woo, S.H. Hwang, S. Yang, S.J. Kim, et al., Effect of IL-10-producing B cells in peripheral blood and tumor tissue on gastric cancer, Cell Commun. Signal. 21 (2023) 320.

[23] R. Wang, C.L. Zuo, R. Zhang, L.M. Zhu, Carcinoembryonic antigen, carbohydrate antigen 199 and carbohydrate antigen 724 in gastric cancer and their relationship with clinical prognosis, World J. Gastrointest. Oncol. 15 (2023) 1475–1485.

[24] J. Li, Z. Chen, Q. Li, R. Liu, J. Zheng, Q. Gu, et al., Study of miRNA and lymphocyte subsets as potential biomarkers for the diagnosis and prognosis of gastric cancer, PeerJ 12 (2024) e16660.

[25] X.-C. Ren, P. Liang, Analysis of influencing factors of nerve invasion in locally advanced gastric cancer, Abdom radiol 48 (2023) 3005–3011.

[26] X. Pan, L. Fu, B. He, J. Hu, W. Zhao, Y. Yang, Using dual-layer detector spectral computed tomography to predict lymph node metastasis and identify differentiation degree of gastric cancer, Researchsquare.com (2022) 1655066.

[27] J. Li, D. Dong, M. Fang, R. Wang, J. Tian, H. Li, et al., Dual-energy CT–based deep learning radiomics can improve lymph node metastasis risk prediction for gastric cancer, Eur. Radiol. 30 (2020) 2324–2333.

[28] F. Giganti, L. Tang, H. Baba, Gastric cancer and imaging biomarkers: part 1–a critical review of DW-MRI and CE-MDCT findings, Eur. Radiol. 29 (2019) 1743–1753.

[29] J. Wu, Y. Lv, N. Wang, Y. Zhao, P. Zhang, Y. Liu, et al., The value of single-source dual-energy CT imaging for discriminating microsatellite instability from microsatellite stability human colorectal cancer, Eur. Radiol. 29 (2019) 3782–3790.

[30] J. Li, M. Fang, R. Wang, D. Dong, J. Tian, P. Liang, et al., Diagnostic accuracy of dual-energy CT-based nomograms to predict lymph node metastasis in gastric cancer, Eur. Radiol. 28 (2018) 5241–5249.

[31] P. Lv, J. Liu, X. Yan, Y. Chai, Y. Chen, J. Gao, et al., CT spectral imaging for monitoring the therapeutic efficacy of VEGF receptor kinase inhibitor AG-013736 in rabbit VX2 liver tumours, Eur. Radiol. 27 (2017) 918–926.

[32] L. Mao, W. Chen, J. Lu, H. Zhang, Y. Ye, Y. Zhang, et al., Quantitative parameters in novel spectral computed tomography: assessment of Ki-67 expression in patients with gastric adenocarcinoma, World J. Gastroenterol. 29 (2023) 1602.

[33] J. Vogel, L. Lin, L. Litzky, A. Berman, C. Simone II, Predicted rate of secondary malignancies following adjuvant proton versus photon radiation therapy for thymoma, Int. J. Radiat. Oncol. Biol. Phys. 99 (2017) 427–433.
[34] J. Li, S. Xu, Y. Wang, M. Fang, F. Ma, C. Xu, et al., Spectral CT-based nomogram for preoperative prediction of perineural invasion in locally advanced gastric cancer: a prospective study, Eur. Radiol. (2023) 1–12.
[35] Q. Zhou, X. Ke, J. Man, B. Zhang, F. Wang, J. Zhou, Predicting masaoka-koga clinical stage of thymic epithelial tumors using preoperative spectral computed tomography imaging, Front. Oncol. 11 (2021) 631649.